AFRL-RV-PS-
TP-2020-0003

AFRL-RV-PS-
TP-2020-0003

ROOM-TEMPERATURE QUANTUM BALLISTIC TRANSPORT IN STRAIN-CONTROLLED NANOWIRE DEVICES

Ashwani Sharma

10 June 2020

Interim Report

AIR FORCE RESEARCH LABORATORY
Space Vehicles Directorate
3550 Aberdeen Ave SE
AIR FORCE MATERIEL COMMAND
KIRTLAND AIR FORCE BASE, NM 87117-5776

DTIC COPY

NOTICE AND SIGNATURE PAGE

Using Government drawings, specifications, or other data included in this document for any purpose other than Government procurement does not in any way obligate the U.S. Government. The fact that the Government formulated or supplied the drawings, specifications, or other data does not license the holder or any other person or corporation; or convey any rights or permission to manufacture, use, or sell any patented invention that may relate to them.

This report is the result of contracted fundamental research which is exempt from public affairs security and policy review in accordance with AFI 61-201, paragraph 2.3.5.1. This report is available to the general public, including foreign nationals. Copies may be obtained from the Defense Technical Information Center (DTIC) (http://www.dtic.mil).

AFRL-RV-PS-TP-2020-0003 HAS BEEN REVIEWED AND IS APPROVED FOR PUBLICATION IN ACCORDANCE WITH ASSIGNED DISTRIBUTION STATEMENT.

//SIGNED//	//SIGNED//
_____	_____
Dr. Ashwani Sharma	Dr. Thomas R. Caudill, Chief
Program Manager/AFRL/RVB	AFRL Battlespace Environment Division

This report is published in the interest of scientific and technical information exchange, and its publication does not constitute the Government's approval or disapproval of its ideas or findings.

Approved for public release: distribution is unlimited.

REPORT DOCUMENTATION PAGE

Form Approved
OMB No. 0704-0188

1. REPORT DATE *(DD-MM-YYYY)*	**2. REPORT TYPE**	**3. DATES COVERED** *(From - To)*
10-06-2020	Interim Report	10 Jun 2019 to 10 Jun 2020

4. TITLE AND SUBTITLE
Room-Temperature Quantum Ballistic Transport in Strain-Controlled Nanowire Devices

5a. CONTRACT NUMBER
In-House

5b. GRANT NUMBER

5c. PROGRAM ELEMENT NUMBER
62601F

6. AUTHOR(S)
Ashwani Sharma

5d. PROJECT NUMBER
4846

5e. TASK NUMBER
EF126848

5f. WORK UNIT NUMBER
V0Y9

7. PERFORMING ORGANIZATION NAME(S) AND ADDRESS(ES)
Air Force Research Laboratory
Space Vehicles Directorate
3550 Aberdeen Avenue SE
Kirtland AFB, NM 87117-5776

8. PERFORMING ORGANIZATION REPORT NUMBER
AFRL-RV-PS-TP-2020-0003

9. SPONSORING / MONITORING AGENCY NAME(S) AND ADDRESS(ES)

10. SPONSOR/MONITOR'S ACRONYM(S)
AFRL/RVBY

11. SPONSOR/MONITOR'S REPORT NUMBER(S)

12. DISTRIBUTION / AVAILABILITY STATEMENT
Approved for public release; distribution is unlimited.

13. SUPPLEMENTARY NOTES

14. ABSTRACT
The findings from the time of flight experiment for strained silicon nanowires are reported in this work, in combination with a numerical simulation demonstrating new physical features involved in the quasi-quantum regime. The drift velocity of valence band holes is demonstrated to exceed greatly that of conduction electrons. These experimental data are accurately reproduced by our simulations, revealing a dramatic reduction in the hole's effective mass as well as a significant increase in the mean-free path between two consecutive random scattering events due to combined effects of quantum confinement and biaxial strain.

15. SUBJECT TERMS
Carrier transport properties in confined structures, strain effects in lattice mismatched interfaces, strained nanowires.

16. SECURITY CLASSIFICATION OF:			**17. LIMITATION OF ABSTRACT**	**18. NUMBER OF PAGES**	**19a. NAME OF RESPONSIBLE PERSON**
a. REPORT	**b. ABSTRACT**	**c. THIS PAGE**			Dr. Ashwani Sharma
Unclassified	Unclassified	Unclassified	Unlimited	28	**19b. TELEPHONE NUMBER** *(include area code)*

This page is intentionally left blank.

TABLE OF CONTENTS

LIST OF FIGURES

In-House Annual Project Report

Title: Room-Temperature Quantum Ballistic Transport in Strain-Controlled Nanowire Devices

PI: Ashwani Sharma, PhD
AFRL/RVBY

Brief Project Description:

Nanowire devices have numerous potential applications in the area of optoelectronics, high-power electronics and RF. Particularly, devices that can deliver high power and operate at very high frequencies while maintaining good signal stability under drastic thermal fluctuations are of particular interest to the AF for GSP applications were linear amplification is required. To achieve ultra-high frequency modulation for broad-bandwidth applications, the amplifier's transistor must be designed to enable high carrier motilities.

The main objective of our proposal was to conduct a first time experimental and theoretical investigation focused on evaluating a new physical phenomena in the quasi-quantum regime in which the hole mobility approached the electron mobility. The hypothesis was based on the fact that a dramatic reduction of the hole's effective mass would occur under the combined effects of two dimensional confinement coupled with strain. The specific conditions (confinement + strain/tensile) for observing this predicted phenomena required a very specific device structure geometry. Our nanowire design consisted of a semiconductor (Si) nanowire core region that was conformably surrounded by slightly lattice mismatched larger-bandgap cladding material (dielectric SiO_2). The Si/SiO_2 lattice mismatch provided the necessary interfacial strain for the experiment. To thoroughly investigate the onset of this phenomenon we had proposed to investigate nanowire core diameters ranging from ~200nm down to ~10nm. The rationale gradually decreasing the crossectional area for the study was based on the fact that the interfacial strain only penetrates a few nanometers into the core region. Therefore in large diameter nanowires, we predicted the strain effects only surrounded the surface of the nanowires and relaxed at the center region atoms (unstrained). Due to the localized Coulomb charges the carriers likely would flowed through the unstrained center region in the larger diameter nanowires. However, as the diameter of the nanowires was reduced the strain closed-in from the both traverse directions, and therefore in the narrowest nanowires (~10nm) the strain conformally penetrated completely through the center, thus ensuring the confined carriers flowed through the strained region. In order to investigate experimentally the optical and electronic properties, the nanowires were configured in a two-terminal metal-semiconductor-metal (MSM) test structure. A metal-Semiconductor/nanowire-metal (MSM) configuration was proposed for this study due to its practicality in photonic and electronic parameter characterization. Characterization for this study included transient time response measurements using a modified version of the Haynes-Shockley experiment for directly evaluating the carrier mobility as a function of nanowire diameter size. Below we provide the results of these experiments with a theoretical model.

Summary of Accomplishments:

In the past year we fully fabricated the nanowire test devices. Si nanowire diameters studied were ~195nm, ~125nm, ~75nm, ~50nm and ~10nm. Figure 1 shows SEM pictures of the crossections of some of the Si nanowire studied that were surrounded by a thermally grown oxide.

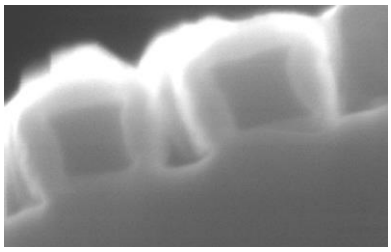

Fig. 1a. Scanning electron microscope (SEM) picture of a wire structures (~195nm) after thermal oxidation.

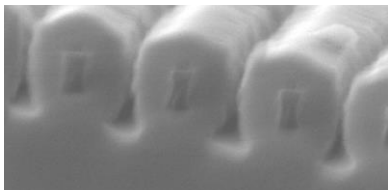

Fig. 1b. Scanning electron microscope (SEM) picture of a wire structures (~75nm) after thermal oxidation.

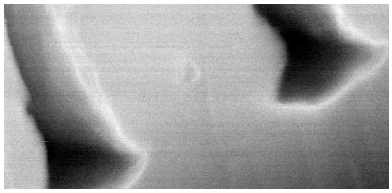

Fig. 1bl. Scanning electron microscope (SEM) picture of a wire structures (~10nm) after thermal oxidation.

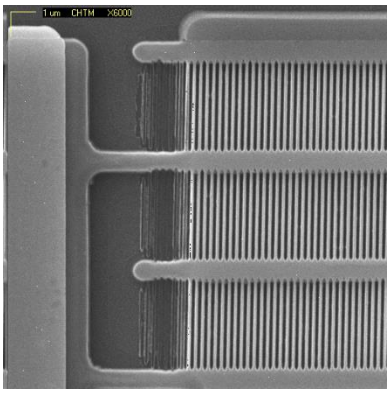
Fig 2a.

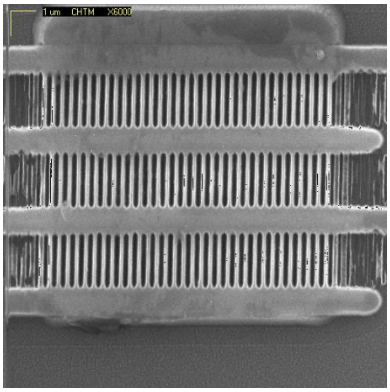
Fig 2b.

Figures 2a and 2b shows a picture of a typical completed device structures active region.

Device characterization experiments (DC current-voltage measurements and Time of flight measurements):

In order to gain insight to the photogenerated carriers and transport properties as a function of dimensional scaling nanowire core region, first dc current-voltage measurements were conducted as follows:

Dark Currents and DC Photocurrents:

The dark current measurements were taken using a digital I-V curve tracer at room temperature. The room lights were turned off to ensure any photogenerated carriers were minimized and would not affect the measurement. The DC photocurrents measurements were conducted at λ=365nm. The laser beam spot was larger than the active area of the nanowire test devices, ensuring carriers were injected uniformly across the sample and provided an optimal signal-to-noise ration. The I-V data below shows the photocurrents measurements. The dark current were negligible and below the resolution of the measuring equipment. The reason the dark currents were extremely small (<<1nA) in these nanowires is due to the fact the nanowires

are basically fully depleted due to the surrounding oxide. The oxide trapped charge, coupled with the interfacial charge resulting from the excess Si atoms not reacted with the oxygen and the mismatch between the number of atomic bonds in the Si crystal surface are sufficient to deplete any carriers from the vicinity. Based on the literature, it is reasonable to expect that the depletion region in the Si nanowire core would extend to a depth of approximately ~40nm from the Si/SiO_2 interfaces. Therefore leaving the entire nanowires fully depleted.

However, once the nanowires were illuminated with a laser spot, the photons striking the nanowire surface, generated electron-hole pairs. The plots below in Figure 3 show the current-voltage characteristics of the nanowires.

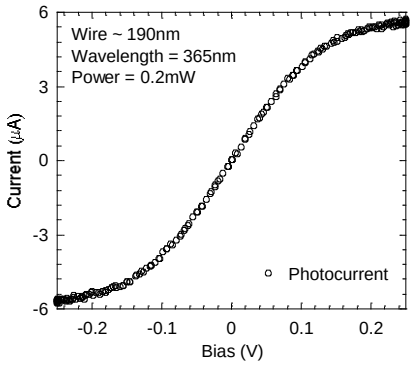

Fig. 3a: ~190nm Si wire MSM device photocurrent-voltage characteristics for 150x150 μm^2 with 8μm gap interdigitated electrodes.

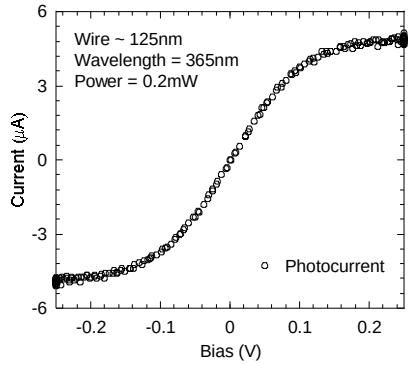

Fig. 3b: ~125nm Si wire MSM device photocurrent-voltage characteristics for 150x150 μm^2 with 8μm gap interdigitated electrodes.

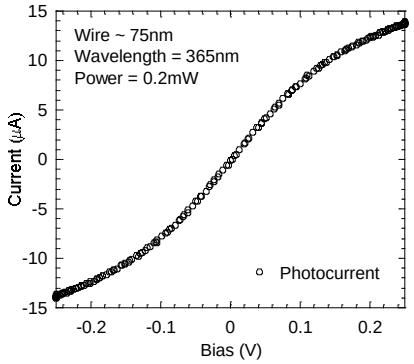

Fig. 3c: ~75nm Si wire MSM device photocurrent-voltage characteristics for 150x150μm^2 with 8μm gap interdigitated electrodes.

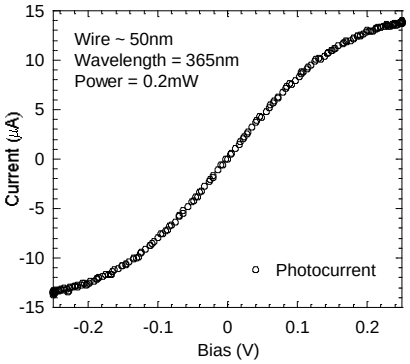

Fig. 3d: ~50nm Si wire MSM device photocurrent-voltage characteristics for 150x150μm^2 with 8μm gap interdigitated electrodes.

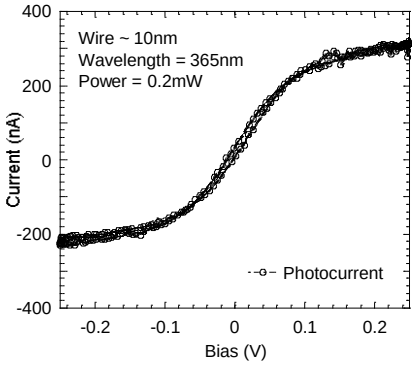

Fig. 3e: ~10nm Si wire MSM device photocurrent-voltage characteristics for 150x150μm^2 with 8μm gap interdigitated electrodes.

From the photogenerated I-V plots above the conductivity values were calculated are plotted below in Figure 4 as a function of nanowire width.

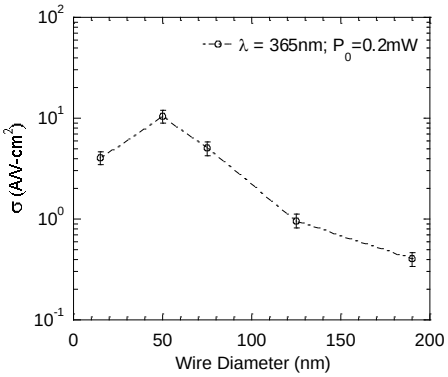

Fig. 4: Plot of conductivity as a function of dimensional scaling the wire diameter.

As can be noticed from the plot above, as the diameter of the nanowire decreased from ~195nm to ~50nm, an increase in the conductivity was observed. The analysis of this observation will be provided in the time of flight section of this report.

Time of flight measurements:

As mentioned earlier the main focus of this proposal was to experimentally investigate the carrier transport phenomenon as a function of scaling the cross-sectional area of the nanowires. The experiment was based on a modified version of the Haynes-Schockley experiment[i]. When carriers are injected at a given place and time, their arrival at another point can be determined. From the measured signal the carrier mobility can be determined. In order to understand the physics of carrier transport a detailed drift-diffusion model was developed in the one-dimension for a pulsed optical signal propagating under an applied electrical field. The experimental carrier mobility results were then compared with this theoretical model in order to gain insight into the transport properties.

Experimental Setup:

Pulsed response measurements were taken using ~150-fs duration excitations at λ=400 nm from a cw mode-locked Ti:Al_2O_3 laser (doubled for the short wavelength, 0.24 mW average power at a 77 MHz repetition rate). The MSM devices were probe tested using an 18 GHz probe and a high-speed digital sampling oscilloscope with a ~1ps resolution capability. The laser spot size was <1 μm in diameter and the electrode gaps were ~8 μm. Normal incidence, TM polarization relative to the structure wavevector was used for the experiment. The time response measurements were taken for low electric field strengths ~$3x10^3$ V/cm, (2.5V across 8 μm gap) thus avoiding velocity saturation and device burnout. See figure 5 below illustrating the setup.

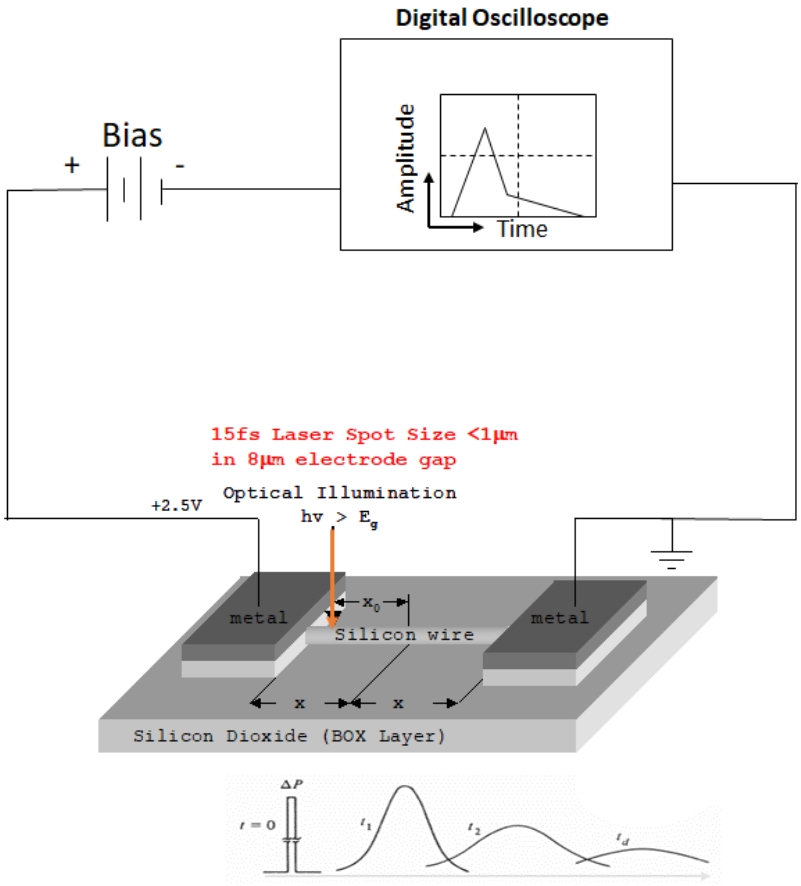

Fig. 5: Schematic of a time response setup configuration.

Experimental Analysis

The experimental time response results for the nanowires are provided below in Figures 6a (signal response) and 6b (rise time vs diameter) along with the theoretically modeled signal. Measurements were taken on each side of the electrodes, by moving the beam spot while maintaining the bias polarity, in attempts to decouple the electron and hole signal components. The electrode fixed bias polarity is positive on the left electrode and the right electrode is ground. With this bias configuration once a pulsed of light with a spot size < 1 μm, as in the case of our experiment, strikes anywhere in the active region, the holes will travel towards the right side electrode and the electrons will travel towards the left side electrode. Figure 5 illustrates the device characterization configuration pictorially with an applied bias of +2.5V.

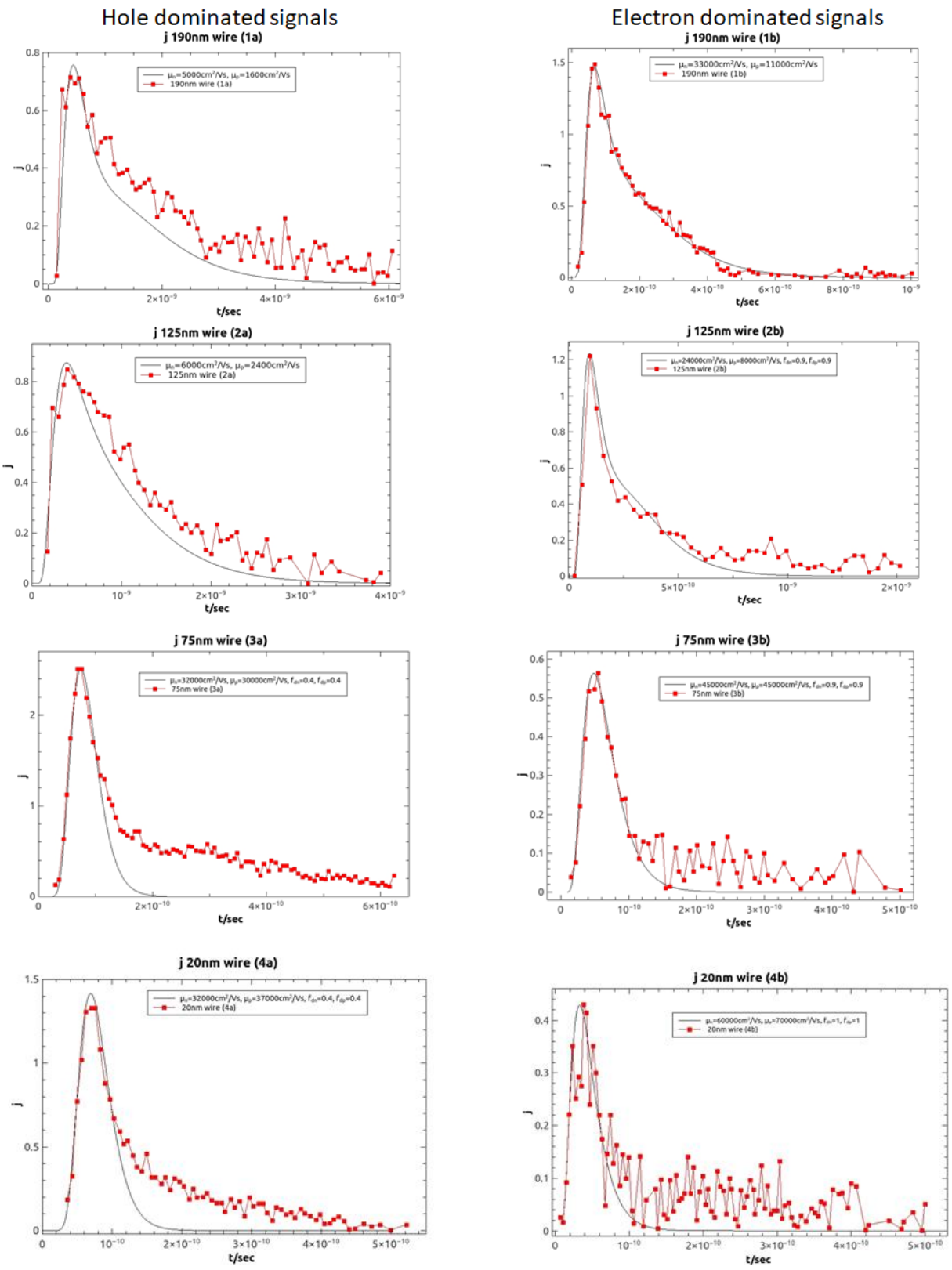

Fig. 6a: Direct time of flight pulsed response measurements.

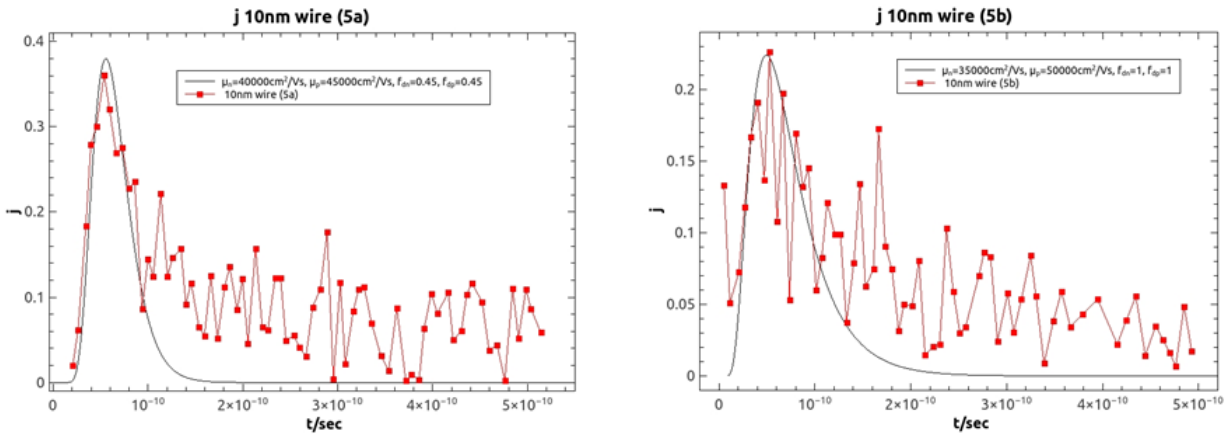

Fig. 6a: (continued) Direct time of flight pulsed response measurements.

Experimental data, we took the rise times of the signals and plotted them as a function of nanowire diameter.

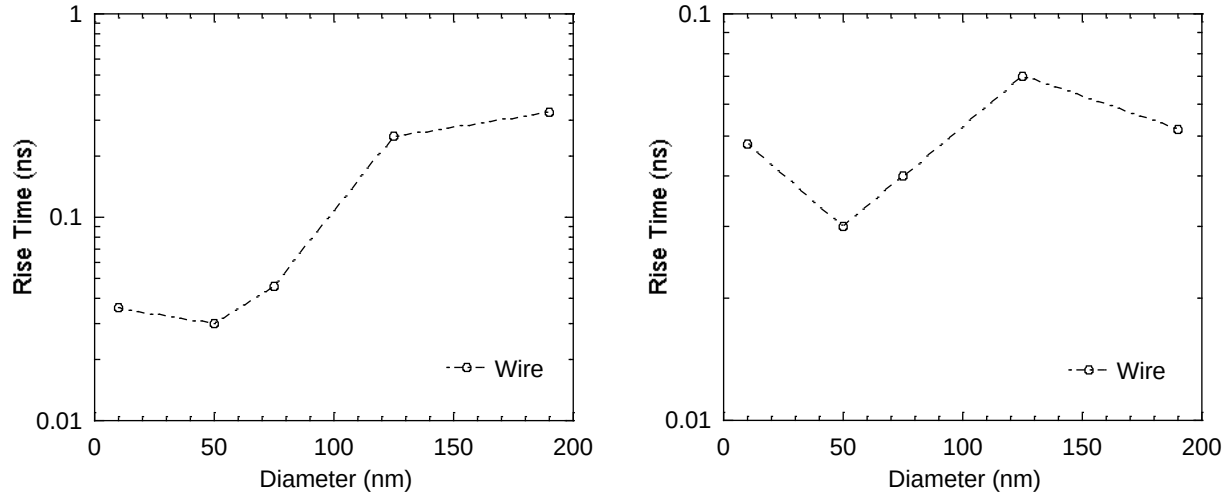

Fig. 6b: Rise time plots as a function of scaling wire diameter (a) left side illumination (hole transport dominant), (b) right side illumination (electron transport dominant).

Experimental and theoretical analysis

From rise-time data nanowires devices we can get insight of the average carrier velocities. For example, for the stated biasing polarity, we know that when the optical pulse is incident upon the left side of the structures the holes move towards the right crossing the entire active region and the electrons towards the left and are collected at the electrode. The width of the measured pulse is therefore is limited due to the hole current. When the optical pulse is incident upon the right side of the structures the width of the pulse can be attributed to the electron current. However in order to better understand the physics of carrier transport we develop a theoretical model to simulate the carrier pulsed responses of the experiment as follows.

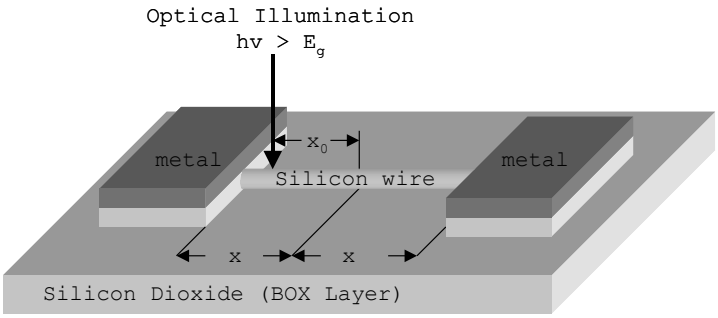

Fig. 7: Schematic of the nanowire devices.

For modeling purposes assume the center of the electrode gap as the origin of the coordinate system and the length of the film, wire or wall is 2x as shown in Fig 7.

We assume that the MSM device is under a constant DC bias. If at time t_0 a narrow pulse of light with a beam spot ~ 1μm << active region length ~ 8 μm strikes within the electrode gap at a distance of x_0 from the center then we generate electron-hole pairs in that region[ii]. At any point within the electrode gap the current consists of drift and diffusion components of current, therefore we use drift diffusion current equation as a first order approximation[iii]. Outside the depletion region the drift component is negligible while current is essentially due to diffusion and inside the depletion region the diffusion current is very small while the carriers are moving under the drift component. To understand the behavior of photo-generated carriers and electric fields in the metal-semiconductor-metal structures[iv], Poisson's equation, and the continuity equation can be solved as follows[v]:

$$\varepsilon\nabla^2\psi = -q(p - n + N_d^+ + N_a^-)$$

$$-\frac{1}{q}\vec{\nabla} J_n + \frac{\partial n}{\partial t} = G_n - R_n$$

$$\frac{1}{q}\vec{\nabla} J_p + \frac{\partial p}{\partial t} = G_p - R_p$$

where, ε is the Permittivity (F/cm^2), ψ is the potential, q it the electron charge (C) , n and p are the electron and hole concentrations (cm^{-3}), N_d^+ and N_a^- are the ionized donor and acceptor impurities contents in the semiconductor (cm^{-3}), J_n and J_p are the electron and hole current densities (A/cm^2),

t is time (s), G_n and G_p are the generation terms and R_n and R_p are the recombination terms for electrons and holes per unit time respectively.

The generation terms G_n and G_p for illumination at one end of the wire can be written as[vi,vii]:

$$G_n = G_p = \frac{P_0\eta}{h\nu} e^{\{-\frac{(x-x_0)^2}{\sigma_x{}^2}\}} e^{\{-\frac{(t-t_0)^2}{\sigma_t{}^2}\}} e^{-\alpha z}$$

where P_0 is the peak optical power density incident upon the surface of the Si wires, $h\nu$ is the photon energy, η is the quantum efficiency, t_0 is the time at which the optical power peaks, x_0 is the x-coordinate of the center of the beam spot, α is the absorption coefficient, z is the penetration depth (for this analysis we ignore the z dependence due to the very small thicknesses of our active region structures), σ_x and σ_t are related to the pulse width FWHM, and $1/e^2$ defined beam diameter D as[viii]

$$\sigma_x = \frac{D}{2\sqrt{2}}$$

and

$$\sigma_t = \frac{FWHM}{2\sqrt{\ln 2}}$$

The recombination rates R_p and R_n are given by[ix]

$$R_n = \frac{n}{\tau_n}$$

and

$$R_p = \frac{p}{\tau_p}$$

where τ_n and τ_p are the electron and hole recombination lifetime.

The electron and hole current densities can be written as

$$J_n = q\mu_n nE + qD_n\nabla n$$

and

$$J_p = q\mu_p pE - qD_p\nabla p$$

where E is the electric field; μ_n and μ_p are the electron and hole mobilities; D_n and D_p are the electron and hole diffusion coefficients. We can rewrite the above equations in terms of drift velocities by substituting $v_n = -\mu_n E$ and $v_p = \mu_p E$ as follows:

$$-J_n = -(-qv_n n + qD_n\nabla n)$$

$$-J_n = qv_n nE - qD_n \nabla n$$

and

$$J_p = qv_p pE - qD_p \nabla p$$

Now we made some substitution and after rearranging we get the following:

$$-v_n \cdot \nabla n - D_n \nabla^2 n + \frac{\partial n}{\partial t} + \frac{n}{\tau_n} = \frac{P_0 \eta}{h\nu} e^{\{-\frac{(x-x_0)^2}{\sigma_x^2}\}} e^{\{-\frac{(t-t_0)^2}{\sigma_t^2}\}}$$

and

$$v_p \cdot \nabla p - D_p \nabla^2 p + \frac{\partial p}{\partial t} + \frac{p}{\tau_p} = \frac{P_0 \eta}{h\nu} e^{\{-\frac{(x-x_0)^2}{\sigma_x^2}\}} e^{\{-\frac{(t-t_0)^2}{\sigma_t^2}\}}$$

To solve the above equations we need find the Green's function for the problem. We can rewrite the above equations as follows:

$$-\nabla^2 n - (\frac{v_n}{D_n})\nabla n + (\frac{1}{\tau_n D_n})n + \frac{1}{D_n}\frac{\partial n}{\partial t} = \frac{S_n}{D_n}$$

and

$$-\nabla^2 p + (\frac{v_p}{D_p})\nabla p + (\frac{1}{\tau_p D_p})p + \frac{1}{D_p}\frac{\partial p}{\partial t} = \frac{S_p}{D_p}$$

where,

$$S_n = S_p = \frac{P_0 \eta}{h\nu} e^{\{-\frac{(x-x_0)^2}{\sigma_x^2}\}} e^{\{-\frac{(t-t_0)^2}{\sigma_t^2}\}} \Rightarrow \text{are the Source Terms}$$

In order to get an expression for the current we have to solve the above equation. For that we need to find the Green's function for the equations,

$$-\frac{\partial^2 n}{\partial x^2} - (\frac{v_n}{D_n})\frac{\partial n}{\partial x} + (\frac{1}{D_n})\frac{\partial n}{\partial t} + (\frac{1}{\tau_n D_n})n = \frac{1}{D_n}\delta(x - x_0)\delta(t - t_0)$$

and

$$-\frac{\partial^2 p}{\partial x^2} + (\frac{v_p}{D_p})\frac{\partial p}{\partial x} + (\frac{1}{D_p})\frac{\partial p}{\partial t} + (\frac{1}{\tau_p D_p})p = \frac{1}{D_p}\delta(x - x_0)\delta(t - t_0)$$

Rewriting n and p as functions of position and time $G_n(x,t)$ and $G_p(x,t)$ respectively,

$$-\frac{\partial^2 G_n(x,t)}{\partial x^2} - \left(\frac{v_n}{D_n}\right)\frac{\partial G_n(x,t)}{\partial x} + \left(\frac{1}{D_n}\right)\frac{\partial G_n(x,t)}{\partial t} + \left(\frac{1}{\tau_n D_n}\right)G_n(x,t) = \frac{1}{D_n}\delta(x-x_0)\delta(t-t_0)$$

and

$$-\frac{\partial^2 G_p(x,t)}{\partial x^2} + \left(\frac{v_p}{D_p}\right)\frac{\partial G_p(x,t)}{\partial x} + \left(\frac{1}{D_p}\right)\frac{\partial G_p(x,t)}{\partial t} + \left(\frac{1}{\tau_p D_p}\right)G_p(x,t) = \frac{1}{D_p}\delta(x-x_0)\delta(t-t_0)$$

Now we take the Fourier Transform of equations,

And we get,

$$K^2 G_n(K,t) - iK\frac{v_n}{D_n}G_n(K,t) + \frac{1}{D_n}\frac{\partial G_n(K,t)}{\partial t} + \frac{G_n(K,t)}{D_n\tau_n} = \frac{1}{D_n}\frac{e^{iKx_0}}{\sqrt{2\pi}}\delta(t-t_0)$$

and

$$K^2 G_p(K,t) + iK\frac{v_p}{D_p}G_p(K,t) + \frac{1}{D_p}\frac{\partial G_p(K,t)}{\partial t} + \frac{G_p(K,t)}{D_p\tau_p} = \frac{1}{D_p}e^{iKx_0}\delta(t-t_0)$$

Since nothing happens for $t<t_0$, we can write $t_0=0$.

Rearranging terms we get,

$$\left(K^2 - iK\frac{v_n}{D_n} + \frac{1}{D_n\tau_n}\right)G_n(K,t) + \frac{1}{D_n}\frac{\partial G_n(K,t)}{\partial t} = \frac{e^{iKx_0}}{D_n\sqrt{2\pi}}\delta(t)$$

and,

$$\left(K^2 + iK\frac{v_p}{D_p} + \frac{1}{D_p\tau_p}\right)G_p(K,t) + \frac{1}{D_p}\frac{\partial G_p(K,t)}{\partial t} = \frac{e^{iKx_0}}{D_p\sqrt{2\pi}}\delta(t)$$

In order to convert the above equations into an algebraic equation we need to take the Laplace Transform which gives,

$$\left(K^2 - iK\frac{v_n}{D_n} + \frac{1}{D_n\tau_n}\right)G_n(K,s) + \frac{s}{D_n}G_n(K,s) = \frac{e^{iKx_0}}{D_n\sqrt{2\pi}}$$

and,

$$(K^2 + iK\frac{v_p}{D_p} + \frac{1}{D_p\tau_p})G_p(K, s) + \frac{s}{D_p}G_p(K, s) = \frac{e^{iKx_0}}{D_p\sqrt{2\pi}}$$

rearranging the left side we get,

$$(K^2 - iK\frac{v_n}{D_n} + \frac{1}{D_n\tau_n} + \frac{s}{D_n})G_n(K, s) = \frac{e^{iKx_0}}{D_n\sqrt{2\pi}}$$

and,

$$(K^2 + iK\frac{v_p}{D_p} + \frac{1}{D_p\tau_p} + \frac{s}{D_p})G_p(K, s) = \frac{e^{iKx_0}}{D_p\sqrt{2\pi}}$$

Now we can write solution of the Green's function for electrons,

$$G_n(K, s) = \frac{\frac{e^{iKx_0}}{D_n\sqrt{2\pi}}}{(K^2 - iK\frac{v_n}{D_n} + \frac{1}{D_n\tau_n} + \frac{s}{D_n})}$$

and holes,

$$G_p(K, s) = \frac{\frac{e^{iKx_0}}{D_p\sqrt{2\pi}}}{(K^2 + iK\frac{v_p}{D_p} + \frac{1}{D_p\tau_p} + \frac{s}{D_p})}$$

Rearranging so we get in standard form we multiply both numerator and denominator by the diffusion coefficient,

$$G_n(K, s) = \frac{1}{\sqrt{2\pi}}\left(\frac{e^{iKx_0}}{D_nK^2 - iKv_n + \frac{1}{\tau_n} + s}\right)$$

and,

$$G_p(K, s) = \frac{1}{\sqrt{2\pi}}\left(\frac{e^{iKx_0}}{D_pK^2 + iKv_n + \frac{1}{\tau_p} + s}\right)$$

We first need to find $G_n(K,t)$, and in order to get that we need to take the inverse Laplace Transform which results as,

$$G_n(K, t) = \frac{e^{iKx_0}}{\sqrt{2\pi}}e^{-(D_nK^2 - iKv_n + \frac{1}{\tau_n})t}$$

and

$$G_p(K,t) = \frac{e^{iKx_0}}{\sqrt{2\pi}} e^{-(D_pK^2 + iKv_p + \frac{1}{\tau_p})t}$$

Which can be rewritten as,

$$G_n(K,t) = \frac{1}{\sqrt{2\pi}} e^{-\frac{t}{\tau_n}} e^{iKx_0} e^{-(D_nK^2 - iKv_n)t}$$

and

$$G_p(K,t) = \frac{1}{\sqrt{2\pi}} e^{-\frac{t}{\tau_p}} e^{iKx_0} e^{-(D_pK^2 + iKv_p)t}$$

To finalize we need G(x,t) which we can get from G(K,t) by taking its inverse Fourier Transform,

$$G_n(x,t) = \frac{1}{2\pi} e^{-\frac{t}{\tau_n}} \int e^{-(D_nK^2 - iKv_n)t} e^{-iKx} e^{iKx_0} dK$$

and

$$G_p(x,t) = \frac{1}{2\pi} e^{-\frac{t}{\tau_p}} \int e^{-(D_pK^2 + iKv_p)t} e^{-iKx} e^{iKx_0} dK$$

Which we can rewrite as,

$$G_n(x,t) = \frac{1}{2\pi} e^{-\frac{t}{\tau_n}} \int e^{-D_nK^2t - iK[(x-x_0) - v_nt]} dK$$

and

$$G_p(x,t) = \frac{1}{2\pi} e^{-\frac{t}{\tau_p}} \int e^{-D_pK^2t - iK[(x-x_0) + v_pt]} dK$$

After solving the integrals and rearranging we get,

$$G_n(x,t) = e^{-t/\tau_n} \sqrt{\frac{1}{4\pi D_n t}} \cdot e^{\frac{-[(x-x_0) - v_nt]^2}{4D_nt}}$$

and

$$G_p(x,t) = e^{-t/\tau_p} \sqrt{\frac{1}{4\pi D_p t}} \cdot e^{\frac{-[(x-x_0) + v_pt]^2}{4D_pt}}$$

The carrier concentrations are calculated as follows,

$$n(x,t) = \int G_n(x,t) S_n dx$$

$$p(x, t) = \int G_p(x, t) S_p dx$$

Since the light pulse was assumed to have a delta function profile, the carrier concentration as a function of position and time are for electrons are reduced to,

$$n(x, t) = \frac{P_0 \eta}{h\nu} \cdot e^{-t/\tau_n} \sqrt{\frac{1}{4\pi D_n t}} \cdot e^{\frac{-[(x-x_0)-v_n t]^2}{4D_n t}} \qquad \text{for } t>0$$

$n(x,t)=0$ for $t<0$

and holes,

$$p(x, t) = \frac{P_0 \eta}{h\nu} \cdot e^{-t/\tau_p} \sqrt{\frac{1}{4\pi D_p t}} \cdot e^{\frac{-[(x-x_0)+v_p t]^2}{4D_p t}} \qquad \text{for } t>0$$

$p(x,t)=0$ for $t<0$

Equations for n(x,t) and p(x,t) show the electron and hole concentration profiles as a function of position and time after for t>0. The equations describe carriers diffusing from the location they are generated due to a gradient. In addition the exponential term containing the drift velocity component shows that if there is a presence of a electric field, then the carriers will also be subject to a drift force in addition to the diffusion. The results describe the physics of the drift and diffusion transport.

In order to calculate the total current density we can write the current density equation as,

$$J_{Total} = q[n(x, t)v_n + p(x, t)v_p - D_n \frac{\partial n(x, t)}{\partial x} - D_p \frac{\partial p(x, t)}{\partial x}]$$

where,

$$\frac{\partial n(x, t)}{\partial x} = \frac{P_0 \eta}{h\nu} \cdot e^{-t/\tau_n} \sqrt{\frac{1}{4\pi D_n t}} \cdot \frac{[(x_0 - x) + v_n t]}{2D_n t} \cdot e^{\frac{-[(x-x_0)-v_n t]^2}{4D_n t}}$$

and

$$\frac{\partial p(x, t)}{\partial x} = \frac{P_0 \eta}{h\nu} \cdot e^{-t/\tau_p} \sqrt{\frac{1}{4\pi D_p t}} \cdot \frac{[(x_0 - x) - v_p t]}{2D_p t} \cdot e^{\frac{-[(x-x_0)+v_p t]^2}{4D_p t}}$$

The above current continuity model was used to analyze the transient time response experimental results for the nanowire devices. The theoretical model was compared with the experimental results by using the rise times (t_d) attained from the experimental data.

$$v_{(Carrier\text{-}Velocity)} = 2x/t_d \text{ (cm/s)}$$

where 2x is the distance between the electrodes (gap) and t_d is the average time it takes for the signal to cross the electrode gap. To better understand the concept of carriers traveling through a semiconductor medium that experience drift and diffusion components,

$$\mu_{avg} = v_{(Avg\,Carrier\text{-}Velocity)}/(V_{bias}/2x)$$

where V_{bias} is the external bias applied to the electrodes.

The equation above can be rewritten as,

$$\mu_{avg} = (2x)^2/(t_d\, V_{bias})$$

After calculating the electron mobility values (μ_n) and the hole mobility values (μ_p) we plotted these values as a function of the nanowire diameters (see Figure 8).

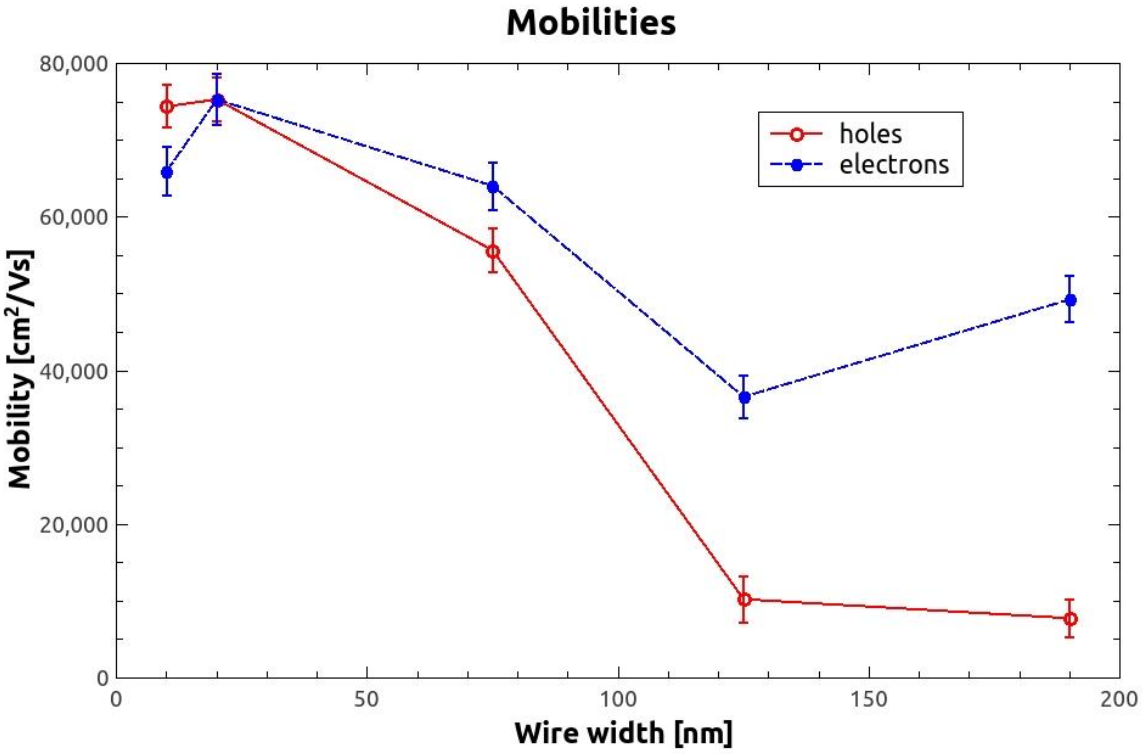

Fig. 8. Electron mobility (blue) and hole mobility (red) plotted as a function of nanowire diameter.

As can be noticed from the plot in Fig. 8, both the electron and hole mobilities tend to increase in a confined nanowire. However, to date no where in literature it has been shown that the hole mobility matches and supersedes the electron mobility. We are the first group to observe this phenomenon and we are currently in the process of theoretically developing a

quantum mechanical model to explain this new phenomenon based on the reversal splitting of light- and heavy- hole bands as well as the decrease of conduction-band effective mass by reduced Si bandgap energy, formulated in a microscopic model for explaining the experimentally observed enhancements in both conduction- and valence-band mobilities in reduced Si nanowire diameters. The role of the biaxial strain buffering depth is elucidated and its importance to the scaling relations, i.e., $1/L^2$ for electrons and $1/L$ for holes. Specifically, the enhancements of the valence-band and conduction-band mobilities are found to be associated with different aspects of the theoretical model.

In order to gain insight to the effects of the competing confinement effects and strain effects, we also conducted photoluminescence experiments. Figure 9 shows the results as follows:

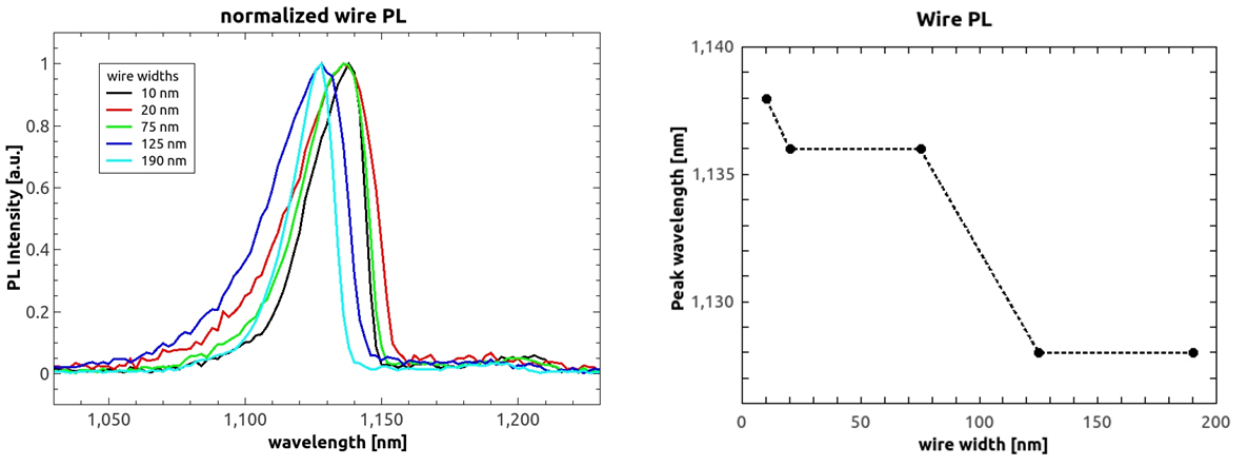

Fig. 9: (a) Measured photoluminescence intensity as a function of wavelength for five Si nanowires with different widths W. (b) Plot of experimentally-extracted photoluminescence-peak wavelength versus W.

The results indicate that although confinement plays a key role in the enhancement of the carrier mobilities, the effects of strain dominate and are responsible, as predicted, for the dramatic reduction in the hole's effective mass values. The reduction in the hole's effective mass is responsible for it's field dependent mobility to surpass the electron mobility.

Proposed Extended Objective:

Based on the observed new physical phenomenon, we believe we are at the point where we have enough experimental data and theoretical model to begin writing a manuscript for potential submission to Physical Review B. This will be done in the next few months.

Publications and Presentations since the Beginning of the Project to Date:

[1] Erin I. Vaughan, Mahmoud Behzadirad, Clay Mayberry, Danhong Huang, and Ashwani K. Sharma, "The Effect on Carrier Transport Properties of Nanostructure Scaling Using Strained, Lattice-Mismatched Semiconductor Interfaces," 59th Electronic Materials Conference, University of Notre Dame, June 28-30, 2017

[2] A. Iurov, G. Gumbs, D. H. Huang, and L. Zhemchuzhna, "Controlling plasmon modes and damping in buckled two-dimensional material open systems", Journal of Applied Physics **121**, 084306(12) (2017).
[3] A. Iurov, G. Gumbs, and D. H. Huang, "Temperature-dependent collective effects for silicone and germanene", Journal of Physics: Condensed Matter **29**, 135602 (2017).
[4] A. Iurov, F. G. Gumbs, Danhong Huang, and G. Balakrishnan, "Thermal plasmons controlled by different thermal-convolution paths in tunable extrinsic Dirac structures", Physical Review B **96**, 245403 (2017).
[5] A. Iurov, L. Zhemchuzhna G. Gumbs, and Danhong Huang, "Exploring interacting Floquet states in black phosphorus: Anisotropy and bandgap laser tuning", Journal of Applied Physics **122**, 124301 (2017).
[6] A. Iurov, G. Gumbs, and Danhong Huang, "Exchange and correlation energies in silicone illuminated by circularly-polarized light", Journal of Modern Optics **64**, 913 (2017).
[7] T.-N. Do, P.-H. Shih, G. Gumbs, Danhong Huang, and M.-F. Lin, "Magneto-electronic Properties of bilayer silicone", Accepted for publication by Physical Review B.
[8] Erin I. Vaughan, M. Behzadirad, D. Huang, and A. K. Sharma, "Improving Carrier Transport in Si/SiO2 Nanowires with Quantum Confinement and Tensile Strain". Submitted to IEEE Nano.

References:

[i] J. R. Haynes and W. Shockley, "The Mobility and Life of Injected Holes and Electrons in Germanium," Phys. Rev., Vol. 81, No. 5, (1951).

[ii] M. B. Ketchen, D. Grischkowshy, T. C. Chen, C.-C. Chi, I. N. Duling, III, N. J. Halas, J.-M. Halbout, J. A. Kash, and G. P. Li, "Generation of subpicosecond electrical pulses on coplanar transmission lines," Appl. Phys. Lett., Vol. 48, pp. 751-753, 1986.

[iii] Eiichi Sano, "A Device Model for Metal-Semiconductor-Metal Photodetectors and its Applications to Optoelectronic Integrated Circuit Simulation", IEEE transactions on electron devices, vol.37, n.9, Sep 1990.

[iv] "Fullwave analysis of picosecond photoconductive switches," IEEE J. Quantum Electron., vol.26, pp. 372-377, 1990.

[v] T. Shah and U. Mishra, "Subpicosecond electrical pulses generation in GaAs by nonuniform illumination of series and parallel transmission line gaps," in OSA Proc. Ultrafast Electron, and Optoelectron., Opt. Soc. Amer., vol. 14, pp. 209-121, 1993

[vi] D. Krokel, D. Grischkowsky, and M. B. Ketchen, "Subpicosecond electrical pulse generation using photoconductive switches with long carrier lifetimes," Appl. Phys. Lett., vol. 54, pp. 1046-1047, 1989.

[vii] E. Sano, "A device model for metal-semiconductor-metal photodetector simulation," IEEE Trans. Electron Devices, vol. 37, pp.1964-1968, 1990.

[viii] Xing Zhou, "Numerical Physics of Subpicosecond Electrical Pulse Generation by Nonuniform Gap Illumination," IEEE JQE, Vol.32, No.9, 1996.

[ix] F. W. Smith, H. Q. Lee, V. Diadiuk, M. A. Hollis, A. R. Calawa, S. Gupta, M. Frankel, D. R. Dykaar, G. A. Mourou, and T. Y. Hsiang, "Picosecond GaAs-based photoconductive optoelectronic detectors," Appl. Phys. Lett., Vol. 54, pp. 890-892, 1989.

DISTRIBUTION LIST

DTIC/OCP
8725 John J. Kingman Rd, Suite 0944
Ft Belvoir, VA 22060-6218 1 cy

AFRL/RVIL
Kirtland AFB, NM 87117-5776 1 cy

Official Record Copy
AFRL/RVB/Dr. Ashwani Sharma 1 cy

This page is intentionally left blank.